Outline of the Unified Theory of Spiral and Bar-like Structures in Galaxies

E. V. Polyachenko*
Institute of Astronomy, Moscow 119017, Russia

Abstract

This paper presents a new approach to studying galactic structures. They are considered as the low-frequency normal modes in a disc of orbits precessing at different angular speeds. Such a concept is an adequate alternative to the commonly used approach of treating the disc as a set of individual stars rotating at near-circular orbits around the centre. The problem of determining the normal modes is reduced to a simple integral equation in the form of the classical eigen-value problem, where the eigen-value is directly equal to the pattern speed of the mode, Ω_p. An examination of the general properties of the basic integral equation shows that two types of solutions exist, bar-like and spiral. The numerical solutions of both types are obtained. The characteristic pattern speeds are of the order of the mean orbit precession speed, although for the bar-modes Ω_p can markedly exceed the maximum precessing speed of orbits. It is shown that the bar-mode grows due to the immediate action of its gravitational field on the stars at the resonance regions. As for the spiral mode, its excitation is probably due to the inner Lindblad resonance that can promote mode growth.

Keywords: Galaxies: structure.

1 Introduction

A disc galaxy is primarily a set of stars which rotate around the centre at near-circular orbits at the angular velocity $\Omega(r)$. The observed spiral and bar-like structures are customarily treated as perturbations in such a differentially rotating disc. Thus, one might expect that the typical pattern speeds of these structures, Ω_p, should be of the order of some average star angular velocity, $\bar{\Omega}$. In reality, however, the pattern speeds Ω_p are of the order of the characteristic precession speed of star orbits, $\bar{\Omega}_{pr}$, which is only a small fraction of $\bar{\Omega}$. Recall that $\Omega_{pr} = \Omega(r) - \kappa(r)/2$ for near-circular orbits, where $\kappa(r) = (4\Omega^2 + \mathrm{d}\Omega^2/\mathrm{d}r)^{1/2}$ is the epicyclic frequency.

According to Lynden-Bell (1979), if stars involved in the formation of the structures satisfy the inequality

$$\epsilon \equiv |\Omega_p - \Omega_{pr}|/\Omega \ll 1, \tag{1}$$

then each star orbit as a whole, but not the individual stars, participates in the perturbations[1]. Consequently, for studying such structures, it is more reasonable to use the model of the disc of star orbits precessing with different speeds than the commonly used concept of the differentially rotating disc of individual stars. The main conjecture of the present paper is that the galactic spirals and bars are the normal modes in such a model of the disc galaxy. In view of its simplicity, this approach, as we will see below, allows one to clarify the underlying physical mechanisms in the formation of galactic structures.

The Lynden-Bell inequality (1) mentioned above are justified by results of numerous calculations (e.g., Athanassoula & Sellwood (1986) for bar-modes or Lin, Yuan & Shu (1969) for spirals).

Fig. 1a shows $\Omega(r)$ and $\Omega_{pr}(r)$ for the Plummer potential $\Phi_0(r) = -(1+r^2)^{-1/2}$ used by Athanassoula & Sellwood (1986) in their N-body bar-mode analysis. The solid thin horizontal line $\Omega_p^{\min} = 0.14$, the dash-dotted line $\Omega_p = 0.21$, and the dashed line $\Omega_p^{\max} = 0.3$ correspond, respectively, to the minimum, mean, and maximum pattern speeds from the list given by Athanassoula & Sellwood (1986) in their Table 1. Fig. 1b represents the ratios $\delta\Omega/\Omega$ ($\delta\Omega \equiv |\Omega_p - \Omega_{pr}|$) for these modes. For the first mode localized inside the circle $r = 2$ (thin dashed lines in Fig. 1b), typical ratios are of the order of 0.1. For the second mode (mean pattern speed), these ratios

*E-mail: epolyach@inasan.rssi.ru

[1]Note, after Arnold (1989), that it was Gauss who had proposed, for studying the perturbations of planets by each other, to smear out a mass of each planet along its orbit in proportion to a time and replace the attraction of planets by the attraction of such rings.

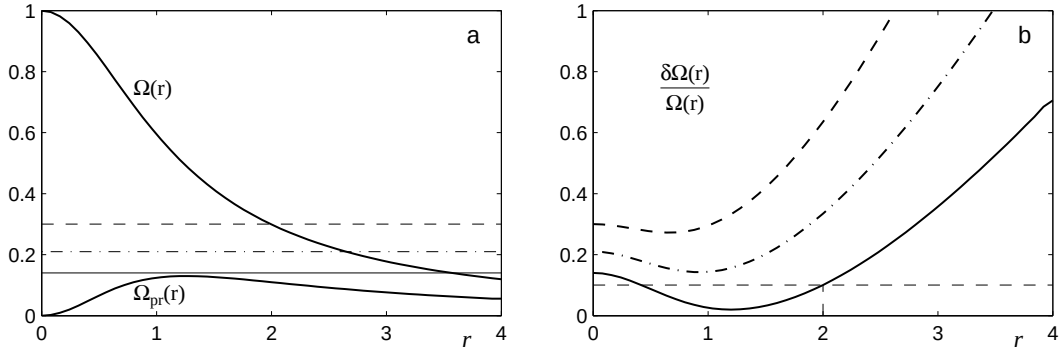

Figure 1: Justification of the Lynden-Bell model of precessing orbits for bar-modes studied by Athanassoula & Sellwood (1986): a) the curves $\Omega(r)$ and $\Omega_{pr}(r)$ for the Plummer potential (thick solid lines), and the minimum, mean, and maximum patterns speeds (thin solid, dash-dotted, and dashed lines, respectively) from the list of Athanassoula & Sellwood (see their Table 1); b) the ratios $\delta\Omega/\Omega$ for Ω_p from a).

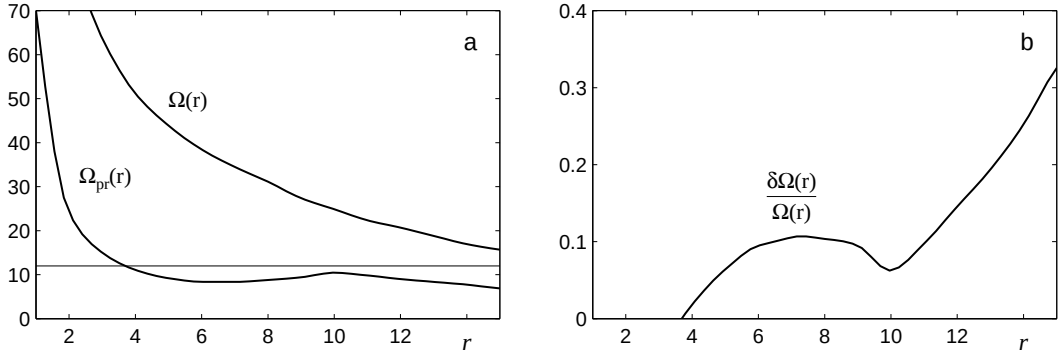

Figure 2: The same as in Fig. 1, for the model of the Galaxy from Lin, Yuan, & Shu (1969).

are typically of the order of 0.2. Even for the fastest mode ($\Omega_p = \Omega_p^{\max}$), typically, $\delta\Omega/\Omega \sim 0.3$, taking into account that this mode is more concentrated to the centre. Therefore it is little wonder that the pattern speeds calculated below (Section 5) in the framework of our approach repeat very accurately those of Athanassoula & Sellwood (1986) in all cases, including the most rapid bar-modes.

On the other hand, it is evident from the curves in Fig. 1b that the inequality (1) and hence our approach fail at sufficiently large radii. This is certainly of no importance for determining the pattern speeds, since the bar-modes are mainly localized near the centre. Roughly speaking, the ratio $\delta\Omega/\Omega$ becomes of the order of 1 near the corotation radius (i.e., at $r_c \approx 3.6, 2.7$, and 2.0, for the first, second, and third modes, respectively).

Fig. 2a,b show similar graphs for the classical spiral example from Lin, Yuan & Shu (1969) where the model of our Galaxy was considered. The pattern speed used here corresponds to the mean of the interval ($\Omega_p = 11 - 13$km s^{-1} kpc^{-1}) suggested in the cited paper, i.e., the horizontal line in Fig. 2a is $\Omega_p = 12$km s^{-1} kpc^{-1}. Fig. 2b shows that the analysis of the eigen-modes of Galactic disc for this model could be performed in the framework of our approach (without the restrictions of the WKBJ theory). Note that substantially higher values of Ω_p, compared to those from Lin et al. (see, e.g., Blitz 1983), are most likely due to an independent peripheral stage of the spiral structure. Such structures can be analyzed using the integral equations described in the end of Section 2.

We picture the disc as comprising a large number of slowly deforming and rotating elliptical rings, along which an individual stars moves so fast it is no more than a blur. Small changes with radius in the shape or orientation of rings give rise to regions of enhanced surface density (see, e.g., Fig 6-11 of Binney & Tremaine 1987). In the absence of self gravity any initial pattern of over-densities will wind up because the part of the pattern at radius r will pecess at a rate Ω_{pr} that varies significantly with r.

Rings that have inclined minor axes exert gravitational torques on one another. These torques cause the angular momenta and radial actions of the rings slowly to change, thus deforming the rings and altering any initial pattern of surface density. The torques also affect the precession rates of the ring's the minor axes. The

interaction between rings is strongest when the rings are physically adjacent, i.e., have similar values of the actions. If we neglect the non-negligible range of the interaction, the disc has something in common with a goods train of deformable wagons connected by springs. Self gravity allows waves of ring deformation to propagate through the disc just as the springs permit waves of wagon displacement and deformation to propagate down the train. We show that these waves can generate a pattern that rotates rigidly at an angular frequency that is larger than the fastest precession rate in the disc.

The picture has points in common with Lynden-Bell's (1979) theory of bar formation in that it focuses on slowly precessing orbital rings, but it does not conclude, with Lynden-Bell, that the bar rotates at a rate that compromises between the fastest and slowest precession rates of the consituent rings. Instead we find that both bars and spirals, in common with many wave phenomena, move faster than the underlying medium. Several studies have shown that the rotation rates of bars in N-body models conform to our predictions rather than those of Lynden-Bell.

The model of precessing orbits can be introduced directly as is done in Section 2 after Eq. (17). However, this model is rigorously justified by the use of the regular procedure of the perturbation theory in the small Lynden-Bell parameter ϵ from (1), with averaging over fast radial oscillations of stars. This programme is implemented in the beginning of Section 2. The resulting integral equations for disc normal modes derived in two ways, namely, (i) directly in the model of precessing orbits, and (ii) with the help of averaging, are identical.

Lynden-Bell (1979) showed that the quantity $J_f = I_1 + I_2/2$ (I_1 and I_2 are the usual actions) is an adiabatic invariant, provided that the inequality (1) is satisfied, i.e., for sufficiently slow perturbations. This means that the orbits evolve by the action of the potential of low-frequency modes only through change in the angular momentum L, with J_f held constant.

Assume that in the initial moment t_0 the distribution function of orbits is $\mathcal{F}_0(J_f, L)$. Let ΔL be a small variation of the orbit angular momentum owing to the action of a small potential perturbation for the time from t_0 to the current moment t. The flow of the phase fluid is incompressible, so the phase element with the initial density $\mathcal{F}_0(J_f, L - \Delta L)$ should come into the point (J_f, L) at the moment t. Accordingly, the Euler differential of the distribution function, i.e., its perturbation, is equal to

$$\mathcal{F} \equiv \mathcal{F}_0(J_f, L - \Delta L) - \mathcal{F}_0(J_f, L) \simeq -\mathcal{F}_0' \Delta L \tag{2}$$

($\mathcal{F}_0' \equiv \partial \mathcal{F}_0(J_f, L)/\partial L$). $\mathcal{F}$ depends on the derivative $\mathcal{F}_0'$. So it is not suprising that just this derivative is found to be critical to our theory of disc slow modes. Henceforth, this derivative is referred to as the Lynden-Bell derivative of the distribution function[2]. It turns out that the behaviour of the Lynden-Bell derivative determines the type of eigen-modes (bar-like or spiral).

To develop the above considerations, immediately resulting from the remarkable paper by Lynden-Bell (1979), into the theory of low-frequency disc modes, one should invoke the dynamical equations and the expression for the 2D disc potential (see Sections 2, 3). As a result, we obtain the integral equations for these eigen-modes (see Eqs. (12) and (16) below). If a potential satisfies these integral equations, the orbits evolve in such a way that the pattern rotates uniformly, with a certain angular speed Ω_p. The physics of our bar-like and spiral solutions consists just in the fact that these are (slow) normal modes. All specificity (compared to general modes) is concerned with their slowness.

The ensuing sections of this paper present the following material. In Section 2, we derive the basic integral equation of the theory (by two methods). The basic integral equation is then reduced to the form of the classical eigen-value problem. Section 3 is devoted to the analysis of the general properties of the basic integral equation. In particular, the crucial role of the Lynden-Bell derivative of the distribution function is revealed. In Section 4, this derivative is examined in more detail by the example of the Schwarzschild model. In two following sections, the specific solutions of the basic integral equation are given. To demonstrate the capabilities of the proposed theory, test models studied earlier by the N-body method (Athanassoula & Sellwood 1986) are adopted (Section 5). The theory gives results in close agreement with results of the N-body simulations. A wide variety of spiral modes are studied in Section 6. In the last Section 7, a brief summary of the results is given.

2 Basic equations

The most convenient variables that should be used under studying the low-frequency modes are $J_f = I_1 + I_2/2$ and $L = I_2$, where J_f is the Lynden-Bell adiabatic invariant (Lynden-Bell 1979), while $(I_1, I_2) \equiv \mathbf{I}$ are the usual actions. The angle variables corresponding to $\mathbf{I}$ are $\mathbf{w} \equiv (w_1, w_2)$. The variables $(J_f, L) \equiv \mathbf{J}$ are also actions, for which $\bar{\mathbf{w}} \equiv (\bar{w}_1, \bar{w}_2) = (w_1, w_2 - w_1/2)$ are the canonically conjugate angles. One can show that for the

[2]When studying the slow bars, Lynden-Bell (1979) has used the same derivative of the star precession speed, $\partial \Omega_{pr}/\partial L$.

unperturbed state

$$\bar{w}_2^{(0)} = \Omega_{pr}(\mathbf{J})t, \tag{3}$$

where t is the time, $\Omega_{pr}(\mathbf{J}) = \Omega_2(\mathbf{J}) - \Omega_1(\mathbf{J})/2$ is the precession speed of the orbit with the actions $\mathbf{J}$, Ω_1 and Ω_2 are the frequencies of star radial and azimuthal oscillations: $\Omega_i = \partial H_0(\mathbf{I})/\partial I_i$ $(i = 1, 2)$, $H_0 = \mathbf{v}^2/2 + \Phi_0(r)$ is the unperturbed star energy expressed in terms of $\mathbf{I}$, $\mathbf{v}$ is the star velocity, $\Phi_0(r)$ is the equilibrium potential. In the limit of near-circular orbits $\Omega_1 = \kappa(r)$, $\Omega_2 = \Omega(r)$, where κ is the epicyclic frequency.

Eq. (3) means that the angular variable $\bar{w}_2$ is slow because $|\Omega_{pr}| \ll |\Omega_1|, |\Omega_2|$. It is easy to show that $\bar{w}_2 = \alpha$, where α is the azimuth of the orbit's minor axis (see below, Fig. 3).

For later use we give here the coordinates of stars r, $\bar{w}_2 - \varphi$, expressed in terms of $\mathbf{J}$, $\bar{w}_1$. The radius $r = r(\mathbf{J}, \bar{w}_1)$ is determined by solving the equation

$$w_1(r, \mathbf{J}) = \Omega_1 \int\limits_{r_{\min}(\mathbf{J})}^{r} \frac{\mathrm{d}r'}{\sqrt{2[E(\mathbf{J}) - \Phi_0(r')] - L^2/r'^2}} \tag{4}$$

(it is assumed that $0 \le w_1 \le \pi$). The slow angular variable

$$\bar{w}_2 = \varphi + \varphi_1(\mathbf{J}, \bar{w}_1), \tag{5}$$

where

$$\varphi_1(\mathbf{J}, w_1) = \Omega_{pr}(\mathbf{J}) \int\limits_{r_{\min}(\mathbf{J})}^{r} \frac{\mathrm{d}r'}{\sqrt{2E(\mathbf{J}) - 2\Phi_0(r') - L^2/r'^2}} - L \int\limits_{r_{\min}(\mathbf{J})}^{r} \frac{\mathrm{d}r'}{r'^2\sqrt{2E(\mathbf{J}) - 2\Phi_0(r') - L^2/r'^2}}. \tag{6}$$

The distribution function $f(\mathbf{J}, \bar{\mathbf{w}}, t)$ is governed by the collisionless Boltzmann equation

$$\frac{\partial f}{\partial t} = [H, f], \tag{7}$$

where H is the Hamiltonian of a star in the self-consistent gravitational field $\phi(\mathbf{r}, t)$,

$$H = \frac{1}{2}\mathbf{v}^2 + \phi(\mathbf{r}, t),$$

$[H, f]$ denotes the Poisson bracket,

$$[H, f] \equiv \frac{\partial H}{\partial \bar{w}_1}\frac{\partial f}{\partial J_f} + \frac{\partial H}{\partial \bar{w}_2}\frac{\partial f}{\partial L} - \frac{\partial f}{\partial \bar{w}_1}\frac{\partial H}{\partial J_f} - \frac{\partial f}{\partial \bar{w}_2}\frac{\partial H}{\partial L}. \tag{8}$$

To linearize the collisionless Boltzmann equation, we assume that

$$f = \mathcal{F}_0(\mathbf{J}) + \mathcal{F}(\mathbf{J}, \bar{w}_1)e^{i(m\bar{w}_2 - \omega t)},$$

$$\phi = \Phi_0(r) + \Phi(\mathbf{J}, \bar{w}_1)e^{i(m\bar{w}_2 - \omega t)},$$

where $\mathcal{F}_0(\mathbf{J}) = f_0(\mathbf{I})$ and $\mathcal{F}(\mathbf{J}, \bar{w}_1)e^{i(m\bar{w}_2 - \omega t)}$ are the unperturbed and perturbed distribution functions, respectively, $\Phi(\mathbf{J}, \bar{w}_1)e^{i(m\bar{w}_2 - \omega t)}$ is the perturbation of the potential, m is the azimuthal wavenumber, ω is the frequency $(\omega = m\Omega_p)$. As a result, we obtain the equation

$$-i(\omega - m\Omega_{pr})\mathcal{F} + \Omega_1\frac{\partial \mathcal{F}}{\partial \bar{w}_1} = \frac{\partial \mathcal{F}_0}{\partial J_f}\frac{\partial \Phi}{\partial \bar{w}_1} + im\Phi\frac{\partial \mathcal{F}_0}{\partial L}. \tag{9}$$

To find the desired low-frequency solutions, one can use the perturbation theory in the small Lynden-Bell parameter ϵ from (1). Let $\mathcal{F} = \mathcal{F}^{(1)} + \mathcal{F}^{(2)} + \ldots$ be the perturbation series in powers of ϵ, so that $\mathcal{F}^{(1)}$ is obtained from (9) by neglecting the terms proportional to Ω_{pr} and $\Phi \propto G$: $\partial \mathcal{F}^{(1)}/\partial \bar{w}_1 = 0$, i.e. $\mathcal{F}^{(1)} = \mathcal{F}^{(1)}(\mathbf{J})$ is an arbitrary function of the integrals of motion, which is subsequently specified by using the periodicity condition for the solution of the next approximation[3].

[3]Since $|\omega - m\Omega_{pr}| \ll \Omega_1$, the wave frequency ω is not determined in the first approximation.

The equation for $\mathcal{F}^{(2)}$ takes the form

$$-i(\omega - m\Omega_{pr})\mathcal{F}^{(1)} + \Omega_1 \frac{\partial \mathcal{F}^{(2)}}{\partial \bar{w}_1} = \frac{\partial \mathcal{F}_0}{\partial J_f}\frac{\partial \Phi}{\partial \bar{w}_1} + im\Phi\frac{\partial \mathcal{F}_0}{\partial L}. \tag{10}$$

Given the periodicity of functions $\mathcal{F}^{(2)}$ and Φ, averaging (10) over $\bar{w}_1$ in the interval $(0, 2\pi)$ yields

$$-(\omega - m\Omega_{pr})\mathcal{F}^{(1)} \approx m\frac{\partial \mathcal{F}_0}{\partial L}\bar{\Phi} \quad (\bar{\Phi} \equiv \frac{1}{2\pi}\int\limits_0^{2\pi} \mathrm{d}\bar{w}_1\, \Phi). \tag{11}$$

The azimuthal number m can take only even values. Formally, it follows from the relation $\exp(im\bar{w}_2) = \exp(imw_2)\cdot\exp(-imw_1/2)$, which remains periodic in w_1 (with a period equal to 2π) only for even m. Physically, a closed precessing orbit is an oval symmetric relative to the centre. So the torque from the perturbations with odd m will break rather than rotate such orbits[4].

Calculating the perturbed surface density,

$$\Sigma = \int \mathrm{d}\mathbf{v}\mathcal{F}^{(1)},$$

and using the expression for the 2D disc potential, we find

$$\Phi(\mathbf{r}) = -G\int \mathrm{d}\mathbf{r}'\frac{\Sigma(\mathbf{r}')}{r_{12}} = -G\int \mathrm{d}\mathbf{r}'\mathrm{d}\mathbf{v}'\frac{\mathcal{F}^{(1)}}{r_{12}},$$

where $r_{12} = [r^2 + r'^2 - 2rr'\cos(\varphi' - \varphi)]^{1/2}$. Now one can change in the last formula from $\mathbf{r}'$, $\mathbf{v}'$ to $\mathbf{J}', \bar{\mathbf{w}}'$ taking into account that $\mathrm{d}\mathbf{r}'\mathrm{d}\mathbf{v}' = \mathrm{d}\mathbf{J}'\mathrm{d}\bar{\mathbf{w}}'$ ($\mathrm{d}\mathbf{J}' = \mathrm{d}J'_f\mathrm{d}L'$, $\mathrm{d}\bar{\mathbf{w}}' = \mathrm{d}\bar{w}'_1\mathrm{d}\bar{w}'_2$):

$$\Phi(\mathbf{J}, \bar{w}_1) = -G\int \mathrm{d}\mathbf{J}'\mathrm{d}\bar{\mathbf{w}}'\frac{\mathcal{F}^{(1)}(\mathbf{J}')\exp[im\delta\bar{w}_2]}{r_{12}},$$

with $\delta\bar{w}_2 \equiv \bar{w}'_2 - \bar{w}_2$. Finally, averaging the potential Φ over $\bar{w}_1$,we obtain the following integral equation[5]:

$$\bar{\Phi}(\mathbf{J}) = \frac{G}{2\pi}\int \mathrm{d}\mathbf{J}'\Pi(\mathbf{J}, \mathbf{J}')\frac{\mathcal{F}'_0(\mathbf{J}')}{\Omega_p - \Omega_{pr}(\mathbf{J}')}\bar{\Phi}(\mathbf{J}'), \tag{12}$$

where $\mathcal{F}'_0 \equiv (\partial\mathcal{F}_0(J_f, L)/\partial L)|_{J_f} = \partial f_0/\partial I_2 - 1/2\partial f_0/\partial I_1$,

$$\Pi(\mathbf{J}, \mathbf{J}') = \int \mathrm{d}\bar{w}_1\mathrm{d}\bar{w}'_1\mathrm{d}\delta\bar{w}_2\frac{\exp(im\delta\bar{w}_2)}{r_{12}}. \tag{13}$$

The function Π can be reduced to the following suitable form:

$$\Pi(\mathbf{J}, \mathbf{J}') = 8\int\limits_0^{\pi} \mathrm{d}\bar{w}_1\cos m\varphi_1 \int\limits_0^{\pi} \mathrm{d}\bar{w}'_1\cos m\varphi'_1\,\psi(r, r'), \tag{14}$$

where

$$\psi(r, r') = \int\limits_0^{\pi} \mathrm{d}\alpha\frac{\cos m\alpha}{\sqrt{r^2 + r'^2 - 2rr'\cos\alpha}}. \tag{15}$$

The function $\Pi(\mathbf{J}, \mathbf{J}')$ (multiplied by the factor $imG/2\pi$) has a meaning of torque acting from the harmonical distribution of orbits, $e^{im\bar{w}'_2}$, with the action $\mathbf{J}'$ to the orbit with the action $\mathbf{J}$ and orientation $\bar{w}_2 = 0$.

[4]It is obvious that the self-consistent perturbations made by such ovals must repeat treir symmetry $\varphi \to \varphi + \pi$, which is valid only for modes with even m. Among them, the bi-symmetric mode $m = 2$ is predominant. For instance, just this bar-mode is most likely the only unstable mode. Indeed, the excees of Ω_p over $(\Omega_{pr})_{\max}$ is due to the self-gravitation. This effect is proportional to the function Π, as it is seen from (16). From (14), it follows that the function Π decreases with m. So, the growth of the modes with $m \geq 4$ owing to CR and OLR would be much less than for the $m = 2$ mode. The ILR resonance for $m \geq 4$, however, will prevent the growth.

[5]The integration over real $\mathbf{J}'$ is correct only for unstable frequencies ($\mathrm{Im}\,\omega > 0$). Thus roots with ($\mathrm{Im}\,\omega < 0$) should be omitted.

It is notable that the integral equation (12) in terms of the function $\mathcal{F}^{(1)}$ has the form of the classical eigen-value problem, where the eigen-value is directly the pattern speed Ω_p. Indeed, determining $\bar{\Phi}$ through $\mathcal{F}^{(1)}$ from (11) and substituting it into (12), one obtains

$$\Omega_p \mathcal{F}^{(1)}(\mathbf{J}) = \int \mathrm{d}\mathbf{J}' K(\mathbf{J},\mathbf{J}') \mathcal{F}^{(1)}(\mathbf{J}'), \tag{16}$$

with the kernel

$$K(\mathbf{J},\mathbf{J}') = \frac{G}{2\pi} \mathcal{F}_0'(\mathbf{J}) \Pi(\mathbf{J},\mathbf{J}') + \Omega_{pr}(\mathbf{J}) \delta[\mathbf{J}-\mathbf{J}']. \tag{17}$$

Eq. (16) is the basic integral equation of the theory.

The integral equation (16) is much simpler than the general integral equations for disc normal modes derived earlier by Kalnajs (1965) and Shu (1970). An ordinary desktop PC is quite capable of solving the integral equation (16).

The most important advantage of the present approach is the fact that it makes clear the underlying physical mechanisms of the instability processes developing in the disc. To reveal these physical mechanisms by using the integral equations of Kalnajs or Shu would be very difficult, and the same is true for the N-body simulations.

The formal derivation of the integral equations (12, 16) for the low-frequency modes of gravitating discs given above is rigorous. However, the physical situation will be more transparent after deriving the equivalent integral equation in another way using explicitly the fact that each orbit as a unit should take part in slow perturbations of interest.

Accordingly, let us consider the distribution function of closed precessing orbits, $f(J_f, L; \alpha, t)$, such that $\mathrm{d}\mathcal{M} = f \mathrm{d}J_f \mathrm{d}L \mathrm{d}\alpha$ is the mass of stars at orbits within a given interval $\mathrm{d}J_f \mathrm{d}L \mathrm{d}\alpha$, α is the azimuth of minor axis, so that the orbit precession speed $\Omega_{pr}(J_f, L) = \dot{\alpha}$. The collisionless kinetic equation for such a distribution function is

$$\frac{\mathrm{d}f}{\mathrm{d}t} = \frac{\partial f}{\partial t} + \Omega_{pr} \frac{\partial f}{\partial \alpha} + M \frac{\partial f}{\partial L} = 0, \tag{18}$$

where one takes into account that $(\partial f/\partial J_f)\dot{J}_f = 0$ for the slow modes of interest (Lynden-Bell 1979), and $\dot{L} = M$, where M is the torque acting on the orbit with given J_f, L, α. Note that such a distribution function f and kinetic equation (18) were earlier suggested by V. Polyachenko (1992).

By linearizing the equation (18) and assuming that $f_1, \bar{\Phi}_1 \propto \exp(-i\omega t + im\alpha)$, one can obtain the equation that is analogous to Eq.(11):

$$-i(\omega - m\Omega_{pr}) f_1 = -M_1 \frac{\partial f_0}{\partial L}, \tag{19}$$

where M_1 is the perturbation of the torque. Let us check that the equations (19) and (11) are actually identical. First of all, it is easy to show that

$$M_1 = -\frac{\partial \bar{\Phi}_1}{\partial \alpha}, \tag{20}$$

where $\bar{\Phi}_1$ is the potential averaged over the selected orbit; this potential is produced by all other orbits of a system:

$$\bar{\Phi}_1 = \bar{\Phi}_1(J_f, L; \alpha) = \frac{1}{\mu} \int_0^l \mathrm{d}s \, \Phi_1(\mathbf{r}) \rho_{lin}^{(J_f, L)}(s), \tag{21}$$

where $\rho_{lin}(s) = 1/v(s)$ is the linear mass density characteristic for each orbit (v is the total star velocity, s is the current length of the orbit, $\mathbf{r}$ is the radius-vector at the orbit), $\mu(J_f, L) = \int_0^l \mathrm{d}s \, \rho_{lin}(s)$ is the mass of stars on the orbit,

$$\Phi_1(\mathbf{r}) = -G \int \frac{\mathrm{d}s' \mathrm{d}\alpha' \mathrm{d}J_f' \mathrm{d}L' \rho_{lin}^{(J_f', L')}(s') f_1(J_f', L'; \alpha')}{\sqrt{r^2 + r'^2 - 2rr' \cos(\varphi - \varphi')}} \tag{22}$$

(φ and φ' are the current azimuths at two orbits).

In the formulae (20) and (21), we used the same notation $\bar{\Phi}$ for the averaged potential as earlier in the derivation of the integral equation (12), since in both cases it was actually the same quantity. To convince oneself that this is correct, one can immediately compare the two expressions for $\bar{\Phi}$, taking into account that a star is within the interval $\mathrm{d}s$ during $\mathrm{d}t = \mathrm{d}s/v_{tot} = \mathrm{d}r/v_r = \mathrm{d}w_1/\Omega_1$. Thereafter it remains to make sure that

the slow angular variable $\bar{w}_2$ and the azimuth α of the minor axis are identical. Indeed, (5) can be rewritten in more informative manner:

$$\bar{w}_2 = \varphi - \Delta\varphi + \Omega_{pr}\Delta t, \tag{23}$$

where Δt is the time it takes for the rotation of a star through the angle $\Delta\varphi$ between the azimuth of the minor axis and the current azimuth φ. Then the identity $\bar{w}_2 = \alpha$ is clear from Fig. 3. After invoking Poisson's equation, we obtain the integral equation that is coincident with Eq. (12).

In addition to the derivations above, let us indicate the simplest way to use Eq. (2) of the Introduction for obtaining the relation (11). The canonical Hamilton equations in variables $(\mathbf{J}, \bar{\mathbf{w}})$ are

$$\begin{aligned} \dot{J}_f &= -\frac{\partial H}{\partial \bar{w}_1}, \quad \dot{I}_2 = -\frac{\partial H}{\partial \bar{w}_2}, \\ \dot{\bar{w}}_1 &= \frac{\partial H}{\partial J_f}, \quad \dot{\bar{w}}_2 = \frac{\partial H}{\partial L}, \end{aligned} \tag{24}$$

where $H(J_f, L; \bar{w}_1, \bar{w}_2)$ is the Hamiltonian. Since the angular variable $\bar{w}_2$ is "slow", for studying the low-frequency modes, the procedure of averaging the equations of motion over a quick variable (in this case, $\bar{w}_1$) is appropriate. As a result, we obtain (see, e.g., Arnold 1989)

$$\begin{aligned} \dot{J}_f &\approx -\frac{1}{2\pi}\int\limits_0^{2\pi} \mathrm{d}\bar{w}_1 \frac{\partial H}{\partial \bar{w}_1} = 0; \\ \dot{L} &\approx -\frac{1}{2\pi}\int\limits_0^{2\pi} \mathrm{d}\bar{w}_1 \frac{\partial H}{\partial \bar{w}_2} = -\frac{\partial \bar{\Phi}_1}{\partial \bar{w}_2}. \end{aligned} \tag{25}$$

The first equations means the adiabatic invariance of J_f, while the second equation determines the evolution of the angular momentum L. Assuming that $\bar{\Phi}$ corresponds to a normal mode, from (25) one can find:

$$\dot{L} = -im\bar{\Phi}\, e^{i(m\bar{w}_2 - \omega t)} = -im\bar{\Phi}\, e^{-i(\omega - m\Omega_{pr})t}.$$

Integrating the last equation over t from $t_0 = -\infty$ to t, we find

$$\Delta L = \frac{m\bar{\Phi}}{\omega - m\Omega_{pr}} e^{-i(\omega - m\Omega_{pr})t}, \tag{26}$$

taking into account that the perturbation is switched off at $t \to -\infty$. Substituting (26) into (2) we obtain (11). It is clear that the perturbed precession speed is the same periodic function of time as ΔL.

Recall that the integral equation (16) is valid only for even m. However, one can obtain the integral equation describing the low-frequency modes for m divisible by m_0 (where m_0 is an arbitrary integer) in the form (16), when replacing

$$\bar{w}_2 = w_2 - \frac{w_1}{2}, \quad \Omega_{pr} = \Omega_2 - \frac{\Omega_1}{2}, \quad \frac{\partial \mathcal{F}_0}{\partial L} = \frac{\partial f_0}{\partial I_2} - \frac{1}{2}\frac{\partial f_0}{\partial I_1}$$

with

$$\bar{w}_2^{(m_0)} = w_2 - \frac{w_1}{m_0}, \Omega_{pr}^{(m_0)} = \Omega_2 - \frac{\Omega_1}{m_0}, \frac{\partial \mathcal{F}_0^{(m_0)}}{\partial L} = \frac{\partial f_0}{\partial I_2} - \frac{1}{m_0}\frac{\partial f_0}{\partial I_1},$$

respectively.

The case $m_0 = 1$ is particularly interesting. The corresponding basic integral equation is suitable for studying low-frequency modes of discs around black holes, in planetary rings, and so forth. Since only two types of the potentials, $\propto r^{-1}$ and $\propto r^2$ are available, in which all orbits have zero precession speeds, there are only two cases ($m_0 = 1$ and $m_0 = 2$) where our approximation that $\bar{w}_1$ is fast is valid in an extensive region.

3 General analysis of the basic integral equation

As it follows from (14), the function Π is real and symmetric: $\Pi(\mathbf{J}, \mathbf{J}')^* = \Pi(\mathbf{J}, \mathbf{J}')$, $\Pi(\mathbf{J}, \mathbf{J}') = \Pi(\mathbf{J}', \mathbf{J})$. Let us restrict ourselves to the regular solutions for the averaged potential $\bar{\Phi}$. Taking into account (11), one can safely divide both sides of (16) by $\mathcal{F}_0'$, multiply by $\mathcal{F}^{(1)^*}$, and integrate over $\mathbf{J}$. Calculating the imaginary part of the resulting equation, one finds

$$(\mathrm{Im}\,\Omega_p) \cdot \int \mathrm{d}\mathbf{J} \frac{|\mathcal{F}^{(1)}|^2}{\mathcal{F}_0'} = 0. \tag{27}$$

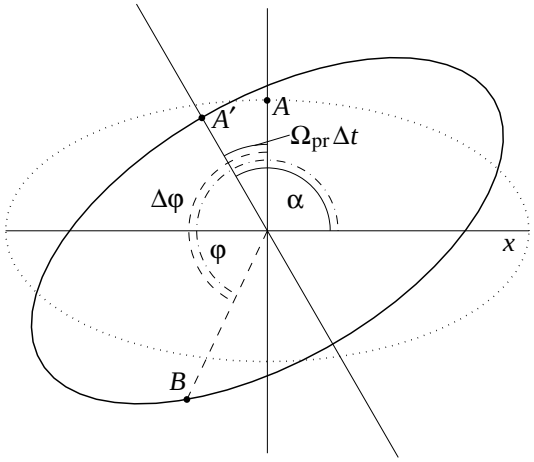

Figure 3: Illustration of the relation (23), which proves the identity $\bar{w}_2 = \alpha$. Dotted and solid ovals show orientations of an orbit at times $t = 0$ and $t = \Delta t$, respectively; the orbit is turned by an angle $\Omega_{pr}\Delta t$. The azimuth of a star initially (at $t = 0$) coincides with the azimuth of the minor axis (point A). The position of the star at $t = \Delta t$ is shown by point B; its azumuth is $\varphi = \widehat{xB}$ (dash-dotted arc), and the variation of the azimuth is $\Delta\varphi = \widehat{AB}$ (dashed arc).

By using (11), Eq.(27) can be reduced to the form

$$(\mathrm{Im}\,\Omega_p) \cdot L_m = 0, \tag{28}$$

where L_m denotes the angular momentum of the mode that can be obtained from the general expression of Lynden-Bell & Kalnajs (1972) retaining the only term which dominates for the low-frequency modes:

$$L_m = -\int \mathrm{d}\mathbf{J} \frac{|\mathcal{F}^{(1)}|^2}{\mathcal{F}_0'} = -\int \mathrm{d}\mathbf{J} \mathcal{F}_0' \frac{|\bar{\Phi}|^2}{|\Omega_p - \Omega_{pr}|^2}. \tag{29}$$

It is found that the type of solution of the basic integral equation depends crucially on the behaviour of the derivative $\mathcal{F}_0'$. Below, we consider two cases.

1. Assume that $\mathcal{F}_0'$ is strictly positive everywhere in the phase space of the system. Then L_m is negative, as well as the energy of the mode δE_m, since $E_m = \Omega_p L_m$ (Lynden-Bell & Kalnajs, 1972). Hence, from (28), one obtains $\mathrm{Im}\,\Omega_p = 0$. The corresponding real eigen-functions, $\mathcal{F}^{(1)}$, describe non-spiral solutions. We identify them with the inner parts of bar-modes, i.e., bars themselves.

Obviously, in the case $\mathcal{F}_0' > 0$ under consideration, the integral equation (16) determines merely the pattern speed $\mathrm{Re}\,\Omega_p$ of a mode. The question now arises of whether there are some external reasons for growth of bar-modes. It is found that the growth can be due to the exchange by the angular momentum with the resonance stars at the corotation and the outer Lindblad resonance (OLR)[6]. These resonances are located rather far from the central regions where the modes are mainly localized. In this respect these resonances are external relative to the modes. Of course, in the end the correctness of our approach is justified by the comparison with results of N-body simulations (see Section 5).

The corresponding growth rate can be calculated by the formula

$$\gamma = \frac{\dot{L}_m}{2L_m}, \tag{30}$$

where $\dot{L}_m = \dot{L}_m^{(1)} + \dot{L}_m^{(2)}$, and the expressions for the rates of exchange by the angular momentum at CR ($\dot{L}_m^{(1)}$) and OLR ($\dot{L}_m^{(2)}$) can be obtained from the general formulas of Lynden-Bell & Kalnajs (1972) through their minor transformation:

$$\dot{L}_m^{(l)} = \frac{1}{4\pi} \int \mathrm{d}\mathbf{J} \left(\frac{l}{2} \frac{\partial \mathcal{F}_0}{\partial J_f} + \frac{\partial \mathcal{F}_0}{\partial L} \right) |\Phi_1^{(l)}|^2 \delta[\Omega^{(l)}(\mathbf{J}) - \Omega_p], \tag{31}$$

[6]If the disc is immersed into the real (but not rigid as in the paper by Athanassoula & Sellwood (1986)) spherical component, one should take into account, generally speaking, the resonance angular momentum exchange between the bar-mode and stars of these component. The dynamical friction caused by resonance interactions of stars of spherical systems with a wave was first studied by Polyachenko & Shukhman (1982).

where δ is the Dirac delta-function, $\Omega^{(l)}(\mathbf{J}) \equiv \Omega_2(\mathbf{J}) + (l-1)\Omega_1(\mathbf{J})/2$, and

$$\Phi_1^{(l)} = -\frac{G}{\pi} \int \mathrm{d}\mathbf{J}' \mathrm{d}\bar{w}_1 \mathrm{d}\bar{w}_1' \psi(r, r') \mathcal{F}^{(1)}(\mathbf{J}') e^{-il\bar{w}_1 + 2i(\varphi_1' - \varphi_1)} \tag{32}$$

is the Fourier coefficient corresponding to CR ($l = 1$) and OLR ($l = 2$) in the expansion of the potential in the series in $e^{il\bar{w}_1}$.

The interaction of stars in the resonance regions with the gravitational potential of the mode leads to the spiral responses. For the corotation resonance, as an example, the response consists of two parts. The resonance response of the disc, without taking its self-gravity into account, produces spirals of angular length about $\pi/2$ (see, e.g., Polyachenko 2002a). The self-gravity also extends the resonance spirals by $\pi/2$ (Polyachenko 2002b). Therefore, the total angular length is about π, which is typical for the majority of SB galaxies (see, e.g., Sandage 1961).

It should be emphasized that above we consider only the linear stage of the formation of structures in SB galaxies. The observed galaxies can have strongly nonlinear bars. The length of such bars is apparently determined by 4:1 resonance. This is exactly the case, e.g., for the nonlinear bar-modes computed by Sellwood & Athanassoula (1987). For a symmetric bar which is free of odd Fourier harmonics, in particular $m = 3$ harmonic, the resonance 4:1 is the nearest to the centre, and thus is the most important one.

2. Let us say that $\mathcal{F}_0'$ becomes negative in some regions of the phase space. For the realistic distribution function (see Section 4), these regions, if they exist, can occupy only a small fraction of the total volume of the phase space. Then, in addition to the fast bars described above, the spiral-like solutions can occur. Contrary to the bars, these new modes grow due to their intrinsic instability, which is inherent to the mode itself. As follows from (28), for an unstable mode ($\mathrm{Im}\,\Omega_p > 0$), the angular momentum $L_m = 0$, i.e. the contributions to L_m from the regions with opposite signs of the Lynden-Bell derivative $\mathcal{F}_0'$ cancel each other exactly: $L_m = L^+ + L^- = 0$. Obviously, the instability is due to the inner Lindblad resonance, since the criterion of instability, $\mathcal{F}_0' < 0$, coincides exactly with the Lynden-Bell & Kalnajs condition of wave exitation at ILR (see (31) when $l = 0$). This resonance becomes the source of spiral waves in the case under consideration, contrary to the commonly accepted view of the role of ILR. Accordingly, the growth rate of the unstable mode can be calculated as

$$\gamma = \frac{\dot{L}^+}{2L^+} = \frac{\dot{L}^-}{2L^-}, \tag{33}$$

where

$$\dot{L}_\pm = \frac{1}{4\pi} \int\limits_{\Gamma_\pm} \mathrm{d}\mathbf{J} \mathcal{F}_0' |\bar{\Phi}|^2 \delta[\Omega_{pr}(\mathbf{J}) - \Omega_p], \tag{34}$$

Γ_+ and Γ_- denote the regions of the phase space with positive and negative values of the Lynden-Bell derivative $\mathcal{F}_0'$, respectively. Note that below the mode growth rates are obtained directly from the solution of the integral equation (16) as $\gamma = 2\mathrm{Im}\,\Omega_p$. However, it is also useful to derive a simple formula for estimate of the growth rate from (33, 34). The simplest case is that with one narrow domain of the negative derivative $\mathcal{F}_0'$. Using the latter equality of (33) and approximating the integrals as the products of the average values of the integrands and small volume of the phase space domain, we obtain:

$$\gamma \simeq |\Omega_{pr}'| \Delta L, \tag{35}$$

where ΔL is the width of the region with $\mathcal{F}_0' < 0$, and $\Omega_{pr}' \equiv \partial\Omega_{pr}/\partial L$ is calculated at the narrow region of the phase space of interest. This estimate is consistent with the explanation of the physical mechanism of the angular momentum exchange at the ILR given by Lynden-Bell & Kalnajs (1972). However, two more points need to be made: (i) the sign of the effect is opposite to that in the cited paper, in accordance with the fact that $\mathcal{F}_0' < 0$, and (ii) strictly speaking, their explanation is appropriate only for the case of near-circular star orbits, although, as we demonstrate below, the very elongated orbits play an essential role. Nevertheless, their considerations can readily be generalized to such a case.

4 Examination of the Lynden-Bell derivative by the example of the typical model

Let us consider the generalized Schwarzschild distribution function (Shu 1970)

$$f_0(E, r_0) = \frac{2\Omega(r_0)}{\kappa(r_0)} \frac{\sigma_0(r_0)}{2\pi c_0^2(r_0)} \exp\left(-\frac{E - E_c(r_0)}{c_0^2(r_0)}\right), \tag{36}$$

where E is the star energy, r_0 is the radius of the guiding centre: $L = r_0^2\Omega(r_0)$, $E_c(r_0) = v_0^2(r_0)/2 + \Phi_0(r_0)$ is the star energy at the circular orbit, $v_0(r_0) = r_0\Omega(r_0)$ is the circular velocity, $\Phi_0(r_0)$ is the equilibrium potential. The specific model is given by the functions $\sigma_0(r_0)$ and $c_0(r_0)$; in the epicyclic limit, when $v_0/c_0 \gg 1$, $\sigma_0(r_0) = \Sigma_0(r_0)$, $c_0(r_0) = c_r(r_0)$, where $\Sigma_0(r_0)$ and $c_r(r_0)$ are the surface density and radial velocity dispersion respectively. In the general case, $\Sigma_0(r_0)$ and $c_r(r_0)$ are expressed by $\sigma_0(r_0)$ and $c_0(r_0)$ in a more complicated manner.

The Lynden-Bell derivative of the distribution function (36) is equal to

$$\frac{\partial \mathcal{F}_0^{(m_0)}}{\partial L} = \frac{2\Omega(r_0)}{r_0^2\kappa^2(r_0)}\mathcal{F}_0\left\{r_0\frac{\Omega'(r_0)}{\Omega(r_0)} - r_0\frac{\kappa'(r_0)}{\kappa(r_0)} + r_0\frac{\sigma_0'(r_0)}{\sigma_0(r_0)} - r_0\frac{2c_0'(r_0)}{c_0(r_0)} + \frac{r_0^2\kappa^3}{2m_0\Omega(r_0)c_0^2(r_0)} + r_0\frac{2c_0'(r_0)}{c_0^3(r_0)}(E - E_c(r_0))\right\}, \quad (37)$$

where $\mathcal{F}_0(\mathbf{J}) = f_0(E(\mathbf{J}), r_0(L))$, a prime denotes the derivative with respect to r_0. As a rule, $\mathcal{F}_0' > 0$ either in all the phase space or at least for the most part (almost everywhere). It is provided by the term $r_0^3\kappa^3/2m_0\Omega c_0^2$ in (37). For example, in the case of the flat rotation curve ($v_0 = \text{const}$), this term equals $(\sqrt{2}/m_0)(v_0/c_0)^2$. Since $v_0/c_0 \gg 1$ almost everywhere in disc galaxies, this term is dominant.

However, there may exist some narrow regions, in which such predominance is broken. Firstly, this is possible in the regions where the function $\kappa(r)$ is sufficiently small. For instance, with a rotation curve similar to that of our Galaxy, such regions can be located at $r \approx 2.5$ kpc and $8 - 10$ kpc. Note the obvious causes of such peculiarities in the rotation curves: (i) a changeover from the potential of the spherical component to the potential of the disc, and (ii) a sharp edge of one of the disc components. Secondly, the function $c_0(r_0)$ increases rapidly when approaching the galactic centre, so that the rotation velocity v_0 in the central parts becomes of the order of c_0.

Relatively small deviations in the behaviour of the rotation curve may lead to very different solutions of the basic equation. Some other factors are also very important. The excess of the pattern speed above the maximum precession rate is due to self-gravity. Thus the solutions have the bar-like form only in sufficiently massive discs, while for discs with relatively small masses we can obtain only spiral modes. The number of very elongated orbits plays the essential role. For example, the excess of such orbits over the number prescribed by the generalized Schwarzschild distribution function (36) strongly increases the growth rate of the spiral modes due to increase of $|\Omega_{pr}'|$ for these orbits. Besides, it is seen from (37) that $|\mathcal{F}_0'|$ ($\mathcal{F}_0' < 0$) increases with $(E - E_c(r_0))$.

5 Numerical test solutions of the basic integral equation

The basic integral equation is studied numerically. The unknown function $\mathcal{F}^{(1)}(\mathbf{J})$ as well as the kernel $K(\mathbf{J}, \mathbf{J}')$ are considered on the 31×31 grid in the phase space (E, L). Then the obtained matrix equation can be solved using standard methods of linear algebra.

It is advisable to put aside the distribution function (36) until the next section and demonstrate the capabilities of the theory by applying it to test models. For such a role, we choose two models investigated by the N-body simulations of Athanassoula & Sellwood (1986). The equilibrium potential for all the models is the Plummer potential, $\Phi_0(r) = -(1 + r^2)^{-1/2}$.

First of all, we are dealing with a Kalnajs (1976) model, which Athanassoula & Sellwood (1986) have denoted by ($m = 6$, $\beta = 0$, $q = 1$, $J_c = 0.25$) (see their Table 1). The computed spectrum of the matrix equation, which consists of 31^2 eigen-values, is shown in Fig. 4. The frequencies are real, since the Lynden-Bell derivative for the Kalnajs models is positive everywhere in the phase space. Just few of eigen-values correspond to the discrete spectrum, while others mimic the continuous part of the spectrum[7], which is the van Kampen – Case modes (van Kampen 1955; Case 1960). They are located in the interval between the minimum and maximum values of the precession speed: $(-0.051, 0.126)$. These modes are the stable solutions of the form $\propto \delta(\mathbf{J} - \mathbf{J}_0)$. The peculiar van Kampen modes are of no interest in studying the bar modes. Thus, in the N-body simulations of Athanassoula & Sellwood, the bar is always one of the modes of discrete spectra. The latter are the eigen solutions of the basic integral equation. Both the perturbed potential and surface density of the discrete modes differ in the number of radial nodes, the nodeless mode being the mode with the maximum pattern speed.

In the spectrum given in Fig. 4 one can see 5 discrete modes. The figure shows that the pattern speeds of the first and second modes (counting from the right) coincide with the pattern speeds obtained in the N-body

[7]The existence of the continuous part of the spectrum is a property of the kernel (17), which defines a bounded noncompact integral operator (*cf.* Reed & Simon 1972).

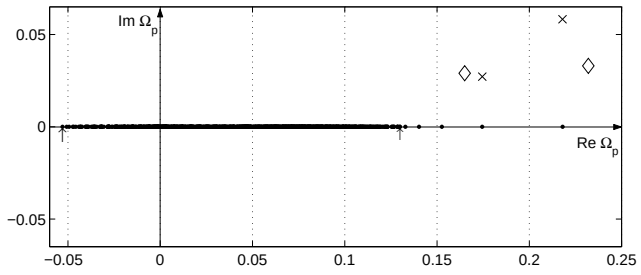

Figure 4: The spectrum of pattern speeds (filled circles) computed as the eigen-values of the problem (16), for one of the Kalnajs models. The crossess are the complex pattern speeds, with the growth rates estimated by the formulas (30), (31). The diamonds are the "experimental" complex pattern speeds according to Athanassoula & Sellwood (1986). The arrows point to the minimum and maximum values of the star precession speed.

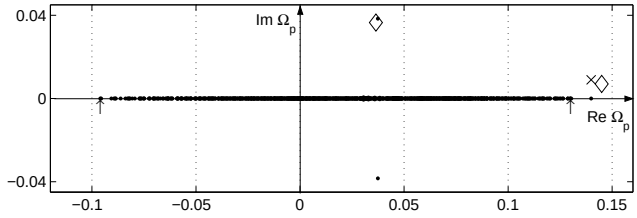

Figure 5: The spectrum of complex pattern speeds (filled circles) computed as the eigen-values of the problem (16), for the model ($m = 6$, $\beta = 3$, $q = 1$, $J_c = 0.6$) of Athanassoula & Sellwood (1986). The cross is the complex pattern speed, with the growth rate estimated by (31). The diamonds are the "experimental" complex pattern speeds according to Athanassoula & Sellwood. The arrows point to the minimum and maximum values of the star precession speed.

simulations to within 6%. It is found (see below) that the growth rates of the other 3 modes are much lower, so they could not be observed in the numerical experiments.

Rough estimates of growth rates for the most rapid modes, in which we assumed that the star orbits are circular, give $\gamma_1 = 0.117$, $\gamma_2 = 0.054$. Each of these values is composed of two parts corresponding to corotation (CR) and OLR: $\gamma_{1CR} = 0.0199$, $\gamma_{1OLR} = 0.0968$, $\gamma_{2CR} = 0.0107$, $\gamma_{2OLR} = 0.0437$. Note that in this case, the OLR terms are dominating. The mode with the maximum pattern speed has the highest growth rate. Obviously, the reason is that such a mode possesses the smallest corotation radius, where the disc surface density is high.

The estimate for the growth rate of the most rapid mode is nearly twise as much as one obtained by Athanassoula & Sellwood (1986) in the N-body simulations. For the second mode, the "experimental" and "theoretical" growth rates are quite close. Among the reasons of the possible discrepancy, one can mention the use of the circular orbit approximation. Recall that the estimates obtained by Athanassoula & Sellwood (1986) within the swing amplification approach are twice as little than their "experimantal" values.

Another model was denoted by Athanassoula & Sellwood as ($m = 6$, $\beta = 3$, $q = 1$, $J_c = 0.6$)[8]. The computed spectrum of eigen-values of bi-symmetric modes for this model, is shown in Fig. 5. The continuous spectrum of van Kampen modes is again located in the interval between the minimum and maximum values of the precession speed: $(-0.096, 0.13)$.

Since the Lynden-Bell derivative for the model under consideration is not positive everywhere in the phase space, the discrete spectrum contains complex modes. In Fig. 5, we can see one unstable complex and one real discrete frequencies. The complex eigen-frequency obtained from the solution of the basic integral equation is very close to the "experimental" frequency, given by Athanassoula & Sellwood (1986). The spiral pattern of the unstable mode is given in Fig. 6.

The pattern speed of the real mode coincides with the pattern speed obtained in the N-body simulations to within 3%. The estimate of its growth rate, in the circular orbit approximation, gives $\gamma = 0.018$, the OLR

[8]The pattern speeds for other models from the list of Athanassoula & Sellwood (1986) were also computed as the eigen-values of the problem (16) (about ten models in all). In all cases the results coincide very closely (with an accuracy of 10% or better). Besides, the eigen-frequencies of the basic integral equation for the isochrone potential coincide within a few percents with those obtained by Kalnajs (1978) using his matrix equation.

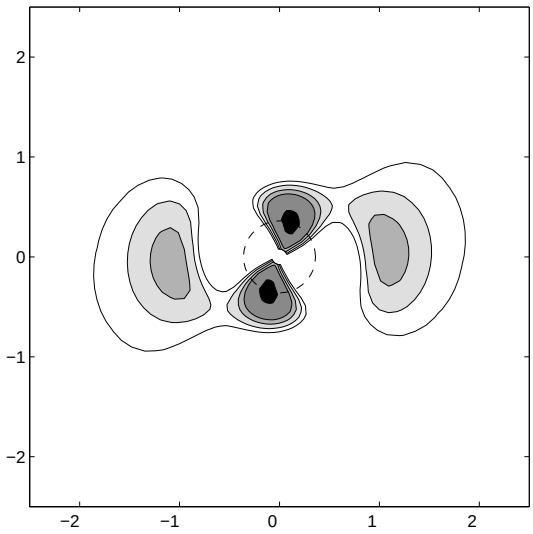

Figure 6: The spiral pattern of the unstable mode in the model ($m = 6$, $\beta = 3$, $q = 1$, $J_c = 0.6$) of Athanassoula & Sellwood (1986). The dashed circle indicates the position of the inner ILR (the outer ILR, for this model, is at $r = 5$).

contribution being dominating. This estimate is 30% larger than that obtained by Athanassoula & Sellwood (1986) in the N-body simulations.

The models explored above are rather artificial. Nevertheless, they were convenient for us because it was thoroughly studied in the N-body simulations by Athanassoula & Sellwood (1986). Besides, the analysis above points to the mechanism of bar-formation in the general case. It is clear that bars can form in galaxies with sufficiently massive discs. In this case, the necessary inequality $\Omega_p > (\Omega_{pr})_{\max}$ can be fulfilled, otherwise the inner Lindblad resonances occur. Then, in the case of a positive Lynden-Bell derivative, only the continuous spectrum of the van Kampen waves exists. Note that the fulfillment of the inequality $\Omega_p > (\Omega_{pr})_{\max}$ is made difficult not only for low-mass discs but also for discs with a high concentration of mass at the centre.

The permitted frequency (pattern speed) of the galactic bar must be one of the eigen-values of the basic integral equation. It means that the corresponding waves remain unchanged over many revolutions of the galaxy, despite the different rates of orbit precession. The half-turn spirals adjacent to the bar form due to the same resonance interaction.

6 Spiral solutions of the basic integral equation

Here we consider in greater detail the situations that arise when the Lynden-Bell derivative is negative in some regions of the phase space. Then a great number of available possibilities appears; they are briefly outlined below. An extended discussion will be published elsewhere.

As a base distribution function for the analysis of the spiral solutions of the basic integral equation, we choose the generalized Schwarzschild distribution function described in Section 4. For the standard model, we assume the "Milky Way-type" rotation curve (see Fig. 7a), and the exponents $\sigma_0(r_0) = \sigma_0 e^{-r_0/r_d}$, $c_0(r_0) = c_0 e^{-r_0/r_c}$ that fix the particular Schwarzschild function. In our units, one kpc is equal to 1, $r_d = 3$, $r_c = 2r_d$, the gravitational constant $G = 1$, $\sigma_0 = (\pi r_d)^{-1}$. The magnitude of the rotation curve is chosen to match the disc component of the velocity curve at radii $r_0 \gtrsim 5$. The maximum rotation velocity is $(v_0)_{\max} = 1.2$, $c_0 \simeq 0.83$, so that for $r_0 = 8$ the ratio $v_0(r_0)/c_0(r_0) \simeq 4$. For such parameters, the galactic disc is exponential almost everywhere, excluding the very central part. Given the rotation curve, the equilibrium potential is $\Phi_0(r) = \int^r \mathrm{d}r'\, v_0^2(r')/r'$. In such a manner we obtain the model of a galaxy, which is similar to our Galaxy (but, of course, the model galaxy is not identical).[9]

Fig. 7c shows the Lynden-Bell derivative, $\mathcal{F}_0'$, for the standard model calculated by (37) at the line of circular orbits ($E = E_{cr}(r_0)$). There is only one narrow region with $\mathcal{F}_0' < 0$ located near the centre. Fig. 8 demonstrates

[9] Remind that the occurrence of the grand design spiral structure in the Galaxy is so far open to question. The galaxies, which we mean in our theory, are more in the nature of NGC 2997 (see, e.g., the image of this galaxy on the cover of the book by Binney & Tremaine (1987).

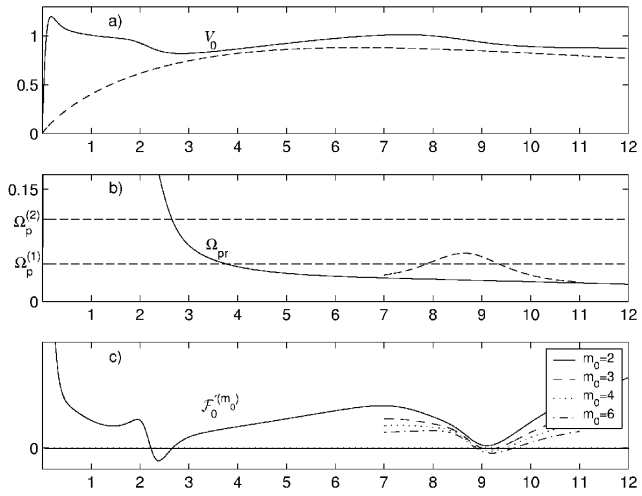

Figure 7: (a) The "Milky Way-type" rotation curve (solid line); dashed line corresponds to the contribution of the exponential disc; (b) The precession speeds, Ω_{pr}, of the circular orbits for the standard model (solid line) and the model with a "peak" near $r = 8-10$ (dashed line). The horizontal straight lines correspond to different pattern speeds; (c) The Lynden-Bell derivatives, $\mathcal{F}_0'^{(m_0)}$, for the circular orbits.

how deep into the phase space the negative values of $\mathcal{F}_0'$ penetrate.

The basic integral equation for the standard model provides a large number of unstable modes. They can be either trailing or leading spirals, the latter are the majority. Narrowly-localized van Kampen solutions of the continuous spectrum, which occupy the wide band of real frequencies, $\Omega_{pr}^{\min} < \Omega_p < \Omega_{pr}^{\max}$, can be both the trailing and leading spirals since for each of these modes, effectively, the gravitational constant $G \to 0$[10]. When employing the concept of eigen-modes, just the packets of leading van Kampen waves participate in the classical swing amplification process described in the original papers by Goldreich & Lynden-Bell (1965), Julian & Toomre (1966), and Toomre (1981). If the dispersion of orbit speeds, $\Delta\Omega_{pr}$, is sufficiently small (that is always assumed), we obtain quasi-monochromatic packets of van Kampen waves. Just such wave packets moving with some group velocity from the central regions and approaching the corotation, can be amplified by the resonance effects under the transformation from the leading form to trailing one. Though each of the van Kampen modes is essentially kinematic ($G \to 0$), the finite packets of these waves are governed by their self-gravity. In particular, the local dispersion relation of Lin–Shu–Kalnajs should be valid for them (away from the resonances).

Here we touch on those improvements, which the present theory can introduce into the original scheme of the swing amplifier. They are connected with the possibility of unstable discrete leading spiral modes. In particular, there is then no need to reflect the short trailing waves somewhere in the central regions to close the feedback loop. Given that the discrete leading modes are monochromatic, the efficiency of the resonance amplification should grow in comparison with quasi-monochromatic packets of the van Kampen waves. These modes might be the "embryo" waves for their subsequent resonance growth due to the swing amplifier. Then, apparently, from the full set of these waves, the mode with the maximum potential perturbation at the corotation is selected. Let us emphasize again the "inversed" role of the ILR (compared to the commonly accepted one), which acts as the generator of spiral waves.

The growth rates of spiral modes for the standard model are rather low: they provide the growth of the amplitude e times, typically for $(3-5)\cdot 10^9$ years (taking into account that $(v_0)_{\max} = 1.2$ corresponds to the rotation period $T = 2.5 \cdot 10^8$ years). The main reason for such low values of growth rates follows from Fig. 8. This figure shows that the curve $\Omega_{pr}(E, L) = \mathrm{Re}\,\Omega_p$ (for a typical unstable spiral mode) intersects the strip of negative values of the Lynden-Bell derivative, $\mathcal{F}_0'$, deep inside the phase space of the system under consideration, at (E, L) corresponding to highly elongated orbits. But the number of such orbits in the Schwarzschild distribution function (decreasing exponentially with the ratio $(E - E_c(r_0))/c_0^2(r_0)$) is small. The growth rates of the spiral modes can be significantly increased if one takes into account that the number of such orbits is actually very much larger. Indeed, we are dealing with the central regions of spiral galaxies, where the contribution of the spherical component, i.e. stars of Population II that have the radially elongated velocity

[10] As computations show, the van Kampen modes are the sole type of solutions for the case when $\mathcal{F}_0' > 0$ everywhere in the galactic disc with the assumed parameters.

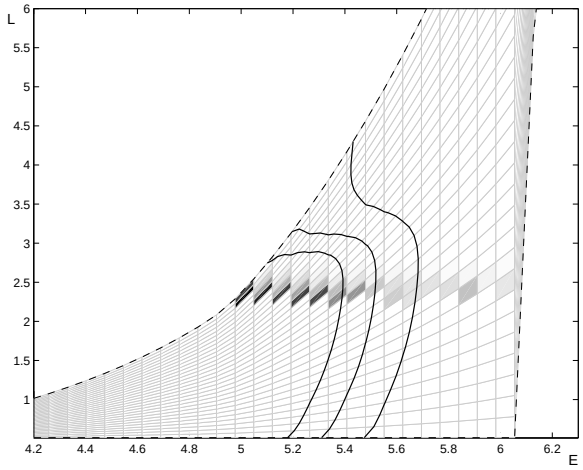

Figure 8: The strip of negative values of the Lynden-Bell derivative, $\mathcal{F}_0'$, at the phase plane (E, L). The phase domain is bounded by the line of circular orbits (from the top) and the line corresponding to $0.02 \cdot (\mathcal{F}_0)_{\max}$, where $(\mathcal{F}_0)_{\max}$ is the maximum value of the distribution function, $\mathcal{F}_0(E, L)$, at each fixed value of E (from the right). The solid curves, $\Omega_{pr}(E, L) = \Omega_p$, indicate the locations of resonance orbits on the phase plane, for several values of Ω_p.

diagram, is essential. It implies that the spherical component can play an important active role, instead of the passive role of a rigid halo as is commonly accepted. Computation with the standard model that is accordingly modified, leads to tenfold growth rates. The modification consists in the substitution $c_0(r_0) \to 2c_0(r_0)$ provided that $(E - E_c(r_0)) > c_0^2(r_0)$. For such a modification, the observed surface density and radial velocity dispersion are almost unchanged. It is also important that this modification leads to the predominance of trailing spiral modes. The observed galactic spirals are most likely just these modes (or similar spirals in other modifications of the standard model). For instance, the modes are most often the trailing half-turn spirals as in the majority of observed galaxies.

In particular, an interesting modification consists of forming the "peak"[11] on the curve Ω_{pr} at sufficiently large r, where the Lynden-Bell derivative can be either positive or negative (in Fig. 8, the upper right corner of the (E, L) phase plane). We omit descriptions of the variety of cases, restricting ourselves to the only picture of the typical spiral mode (Fig. 9).

In conclusion let us touch on one very important aspect of the problem. Fig. 7c shows that the "generalized" Lynden-Bell derivative $\mathcal{F}_0'^{(m_0)}$ at $m_0 > 2$ can be made negative more easily compared to the case $m_0 = 2$. This effect is due to the inverse dependence of the large positive term $r_0^2\kappa^3/2m_0\Omega c_0^2$ in the expression (37) on m_0. Hence, in the outer parts of galaxies (for our Galaxy, just beyond the Solar circle) the additional multi-arm structures are generated, which are independent from the central spiral structure (the latter usually has two arms)[12]. Furthermore, one can expect that several modes will be generated there simultaneously leading to formation of the so-called flocculent structures (Elmegreen & Elmegreen 1982, 1987). All the aforementioned agrees with observations of galaxies (see, for example, The Hubble Atlas of Galaxies, Sandage (1961)). As a rule, in the central part of the disc, the regular two-arm spiral is seen, which is then superseded by a multi-arm or disordered structure. It is appropriate to mention here that Elmegreen (1992) has clearly demonstrated that three-arm spiral structures appear only on the periphery of galaxies beyond the inner Lindblad resonance for the $m = 3$ mode.

7 Discussion

The new approach to the study of structures in spiral galaxies suggested above is based on a view of a galactic disc as a set of precessing orbits. Following this model, we have obtained the simple integral equation that is a very convenient tool for studying galactic structure. Non-axisymmetric structures are considered as the normal

[11] For our Galaxy, such a "peak" has been marked since the well-known paper by Lin, Yuan, & Shu (1969).

[12] The curves $\mathcal{F}_0'^{(m_0)}(r)$ in Fig. 7c are shown only at sufficiently large radii to emphasize that modes with $m_0 > 2$ cannot typically occupy as wide a region as the two-arm mode does. This is explained by the different behaviour of $\Omega_{pr}(r)$ and $\Omega_{pr}^{(m_0)}(r)$ for $m_0 > 2$.

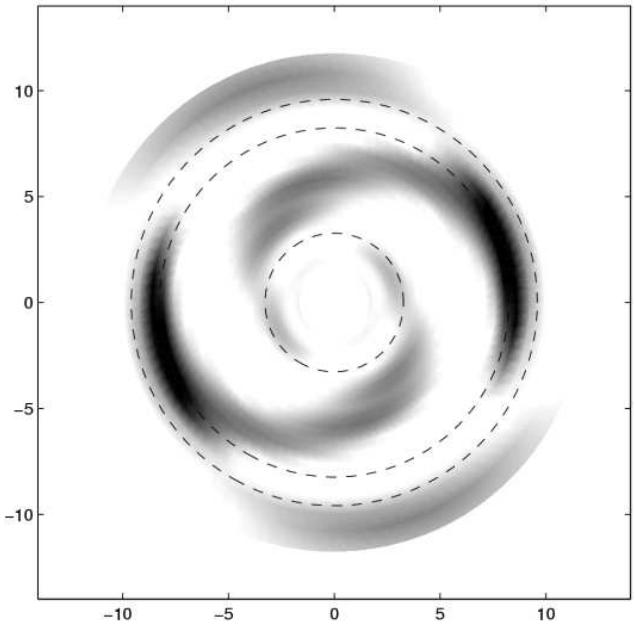

Figure 9: One of typical pictures of unstable spiral modes.

modes of the basic integral equation (16). It is found that the properties of solutions depend crucially on the behaviour of the Lynden-Bell derivative, $\mathcal{F}_0'$, at the phase space of the disc. The solutions have bar-like or spiral form depending on whether $\mathcal{F}_0'$ is positive everywhere or negative somewhere in the phase space.

Within the framework of the suggested approach, which does not include the swing amplifier, we succeeded in calculating the pattern speeds and growth rates of all the modes obtained earlier in the N-body simulations by Athanassoula & Sellwood (1986), the coincidence of results being very high.

Thus, it is shown that the bar-mode grows due to the immediate action of its gravity on the stars in the vicinity of corotation leading to the angular momentum exchange between these stars and the bar-mode. Note that Athanassoula & Sellwood (1986) could readily calculate exact growth rates of all the modes they computed by the formulas (30, 31). However, they preferred the language of swing amplification for rough estimates of the growth rates.

To avoid confusion, we should emphasize that here we deal only with the standard fast bars. As for the slow bars of Lynden-Bell (1979), they are most likely the central parts of the unstable spiral modes (in this sense, they are secondary). Note that here we leave aside the possibility of the slow bar formation in very hot centres of galactic discs (in full analogy to the ellipsoidal deformation of spherical systems under the action of the radial orbit instability). In contrast, the fast bars are primary while the adjacent spirals are secondary since the spirals form as the response of the disc near the corotation to the bar gravity.

The commonly used approach to the problem of formation of the normal spiral structures consists in using either the swing amplification mechanism (Toomre 1981) or its weaker counterpart (overreflection with reference to the waser mechanism – see, e.g., Bertin & Lin 1996). Note that the swing amplification mechanism is sometimes the only way for growth of the initial perturbations. It seems likely that such galaxies do not have any organized spiral structure of the mode nature. Certainly, this mechanism can effectively amplify transient wave perturbations.

In traditional mechanisms, the region of corotation plays the central role. In our approach, we draw attention to ILRs that can under certain conditions cause the excitation of a great variety of spiral modes. Unlike the usual epicyclic idea of ILR as a certain circle, ILR in our unstable modes extends over wide regions of the galactic disc. This is due to participation of a variety of orbits including highly elongated orbits (see Fig. 8). On the one hand, ILR can give rise to leading spiral modes, which in turn can be the "embryos" for further work of the swing amplifier. On the other hand, ILR can provide a variety of trailing spirals including those in the region between two ILRs (see Fig. 7b).

Acknowledgments

With thanks to V.L. Polyachenko for useful discussions.

Appendix. Some additional arguments in support of the used approach

1. The perturbed distribution function f is represented as a Fourier series that contains resonance denominators:

$$f \sim \sum_l \frac{a_l\, e^{ilw_1}}{(\omega - m\Omega_2) + l\Omega_1}. \tag{38}$$

It is natural to name the terms with $l = -1$, $l = 0$, and $l = 1$ as "ILR", "CR", and "OLR" terms, respectively. In Section 2, we have restricted ourselves to the only ILR term. As it was shown in Section 4, this leads to the correct results (with an accuracy of 10%) in determination of the pattern speeds. Thus, one can conclude that the ILR-term has a dominant role.

2. The ratio of the denominator of the ILR term to the denominator of the CR term (closest to ILR) is

$$A = \frac{|\omega - m\Omega_{pr}|}{|\omega - m\Omega_2|} = \frac{\delta\Omega}{|\Omega - \Omega_p|}, \tag{39}$$

where the quantity $\delta\Omega = |\omega - m\Omega_{pr}|$ was already used in the Introduction. Strictly speaking, this ratio is equal to the Lynden-Bell small parameter ϵ from (1) only when $|\Omega| \gg |\Omega_p|$, i.e. in the central regions far enough from the corotation. Fig. 10 shows the ratio (39) for the same 3 models as in Fig. 1. It is seen that $A \ll 1$ for the slowest mode, so the validity of the theory is justified for such modes. The fact that the theory has a certain field of application justifies the main conclusions of the theory (classification of modes, physics of instabilities), derived in Section 3. They can be adequate even beyond the framework of rigorous validity of our approximate theory. For the other two modes from Fig. 10, the ratio is considerably smaller than 1 only in the central regions. Nevertheless, we can hope that the approach is still valid even for these modes, at least quantitatively, taking into account that the perturbation amplitude decrease with radius, being relatively small at the corotation. Besides, there is one more factor that weakens the role of CR term; it is considered in the next point.

3. The coefficient a_l in the expansion (38) is proportional to the linear combination of the derivatives of the unperturbed distribution function $f_0(\mathbf{I})$ (see below, item 5):

$$a_l \sim f'_{0,lm}(\mathbf{I}), \tag{40}$$

where

$$f'_{0,lm}(\mathbf{I}) = l\frac{\partial f_0(\mathbf{I})}{\partial I_1} + m\frac{\partial f_0(\mathbf{I})}{\partial I_2}. \tag{41}$$

Thus, for the bi-symmetric mode $m = 2$ one should actually calculate the ratio

$$A' = \frac{f'_{0,02}(\mathbf{I})}{|\omega - m\Omega_2|} : \frac{f'_{0,-12}(\mathbf{I})}{|\omega - m\Omega_{pr}|}, \tag{42}$$

rather than (39). In the epicyclic approximation, which is valid everywhere beyond the very central parts of galactic discs:

$$\left|\frac{\partial f_0}{\partial I_1}\right| \gg \left|\frac{\partial f_0}{\partial I_2}\right|. \tag{43}$$

Fortunately, for the CR term $l = 0$, so the ratio (42) contains the additional small factor (compared to (39)). Apparently, this may be very important for explaining why our theory is valid even for fastest modes.

4. Intuition suggests that higher harmonics (with $|l| \geq 2$) cannot considerably influence the large scale modes, which are the subject of our study. The particular number of harmonics, needed for the mode computation, is determined "experimentally". The comparison with N-body simulations shows that the only ILR term provides a reasonable accuracy. In the next point we give a more detailed analysis of the relative roles of the terms in the expansion (38).

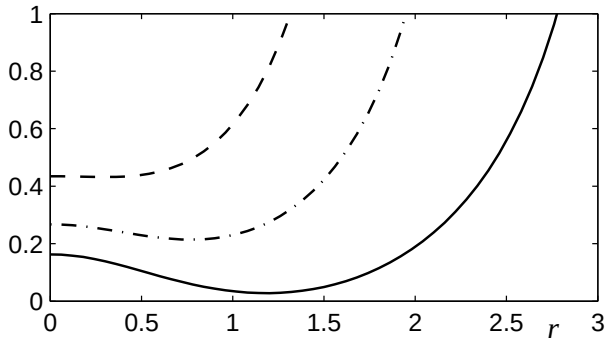

Figure 10: The ratio $A(r)$ for different values of the pattern speed Ω_p: solid, dash-dotted, and dotted lines correspond to the minimum ($\Omega_p^{\min} = 0.14$), mean ($\bar{\Omega}_p = 0.21$), and maximum ($\Omega_p^{\max} = 0.3$) pattern speeds, respectively.

5. Let us derive the generalization of the basic integral equation that takes into account all a resonanses of the perturbation with fixed azimuthal number m. Let the perturbed potential and the perturbed distribution function are expanded in Fourier series

$$\Phi(\mathbf{I}, w_1) = \sum_l \Phi_l(\mathbf{I}) e^{ilw_1}, \qquad f(\mathbf{I}, w_1) = \sum_l f_l(\mathbf{I}) e^{ilw_1}, \tag{44}$$

where $\mathbf{I} = (I_1, I_2)$ are usual radial and azimuthal actions, w_1 is the radial angular variable. Substituting the full potential and the full distribution function

$$\Phi_0 + \Phi(\mathbf{I}, w_1) e^{imw_2}, \qquad f_0 + f(\mathbf{I}, w_1) e^{imw_2}, \tag{45}$$

into the collisionless Boltzmann equation, one can obtain after linearization

$$f_l(l\Omega_1 + m\Omega_2 - \omega) = \Phi_l f'_{0,lm}, \tag{46}$$

where the function $f'_{0,lm}$ is

$$f'_{0,lm}(\mathbf{I}) = l\frac{\partial f_0(\mathbf{I})}{\partial I_1} + m\frac{\partial f_0(\mathbf{I})}{\partial I_2}. \tag{47}$$

The second relation between $\Phi_l(\mathbf{I})$ and $f_l(\mathbf{I})$ is provided by the Poisson equation

$$\Phi(\mathbf{I}, w_1) e^{imw_2} = -G \int \mathrm{d}\mathbf{I}' \mathrm{d}\mathbf{w}' \frac{f(\mathbf{I}', w'_1) e^{imw'_2}}{r_{12}}. \tag{48}$$

Multiplying both sides of the equation by $e^{imw_1/2}$ and introducing function

$$\varphi_1(w_1) = w_2 - w_1/2 - \varphi \tag{49}$$

(see Section 2), one can obtain

$$\sum_l \Phi_l(\mathbf{I}) e^{i(l+m/2)w_1} = -G \int \mathrm{d}\mathbf{I}' \mathrm{d}w_1 \sum_{l'} f_{l'}(\mathbf{I}') e^{i(l'+m/2)w'_1} e^{im\delta\varphi_1} \psi(r, r'). \tag{50}$$

where $\delta\varphi_1 = \varphi'_1 - \varphi_1$. Denoting $\Pi_{l,l'}$ the integral

$$\Pi_{l,l'}(\mathbf{I}, \mathbf{I}') = \int \mathrm{d}w_1 \mathrm{d}w'_1 \psi(r, r') e^{i(l'+m/2)w'_1 - i(l+m/2)w_1} e^{im\delta\varphi_1}, \tag{51}$$

one obtains the second relation:

$$\Phi_l = -\frac{G}{2\pi} \int \mathrm{d}\mathbf{I}' \Pi_{l,l'}(\mathbf{I}, \mathbf{I}') f_{l'}(\mathbf{I}') \tag{52}$$

(here and below the summation over the blind index l' is assumed). Thus, expressing f_l from (46) one can derive the final set of integral equations:

$$\Phi_l(\mathbf{I}) = -\frac{G}{2\pi} \int \mathrm{d}\mathbf{I}' \Pi_{l,l'}(\mathbf{I}, \mathbf{I}') f'_{0,l'm}(\mathbf{I}') \frac{\Phi_{l'}(\mathbf{I}')}{l\Omega_1 + m\Omega_2 - \omega} \tag{53}$$

For numerical calculations, it is more convinient to rewrite the equation (53) in the form of the classical eigen-value problem. Indeed, using (46) one can obtain

$$f_l(\mathbf{I})(l\Omega_1 + m\Omega_2 - \omega) = -\frac{G}{2\pi} f'_{0,lm}(\mathbf{I}) \int \mathrm{d}\mathbf{I}' \Pi_{l,l'}(\mathbf{I}, \mathbf{I}') f_{l'}(\mathbf{I}') \tag{54}$$

Using the discretization of the integrals $\int \mathrm{d}\mathbf{I}' \to \sum \Delta\mathbf{I}'$, the eigen-frequencies can be obtained from the condition:

$$\det \left| \frac{G}{2\pi} f'_{0,lm}(\mathbf{I}) \Pi_{l,l'}(\mathbf{I}, \mathbf{I}') \Delta\mathbf{I}' + \mathbf{E}(l\Omega_1(\mathbf{I}) + m\Omega_2(\mathbf{I}) - \omega) \right| = 0, \tag{55}$$

where $\mathbf{E}$ is the unity matrix. Note that the basic integral equation (16) is the special case of (54) when $l = l' = -1$.

In fact, the equations (54, 55) give a new formulation of the general eigen-value problem for galactic discs. This formulation can be considered as an alternative for the well-known matrix approach of Kalnajs (ApJ, v.212, p.637 (1977)).

Let us employ the equation (55) to define more exactly the eigen-frequencies of the bi-symmetric $m = 2$ modes in the Kalnajs model $(6, 0, 1.0, 0.25)$, which was already studied in Section 4. Athanassoula & Sellwood reported that there are two unstable bar-modes: $\omega_1 = 0.465 + 0.066i, \omega_2 = 0.33 + 0.058i$. We found that for this model the Lynden-Bell derivative is positive everywhere, so only bar-modes with $\Omega_p > (\Omega_{pr})_{\max}$ were possible. Using the basic integral equation (16), we can determine only the pattern speed of the modes; they found to be $\mathrm{Re}\,\omega_1 = 0.44$, $\mathrm{Re}\,\omega_2 = 0.35$. We argued that the growth rate for these modes can be obtained, taking into account the angular momentum exchange at the resonances (primarily, CR and OLR). Rough estimates gave us $\gamma_1 = 0.117$ and $\gamma_2 = 0.054$; notably, the OLR contribution were dominating in both cases.

Restricting ourselves to consideration of three terms with $|l| \le 1$ in the set of equations (54), we can study the impact of three main resonances: ILR, CR, and OLR. First of all, we obtained the unstable bar-modes, when all three terms are present (run 1). Then, the influence of a particular resonance can be "measured" separately by omitting an unnecessary term. In such a way, we study the influence of CR term, switching off the OLR term (run 2). After that we study the impact of the OLR term, omitting CR term (run 3). In all these three cases, when the principal ILR term is present, the pictures of the unstable modes in the complex ω-plane resemble each other. The situation has changed when we dropped the ILR term. In the result we obtained unrealistic picture of a sea of unstable modes with growth rates less than $7 \cdot 10^{-4}$. This fact certainly confirms the dominating role of the ILR term.

The computed eigen-frequencies are given in the table.

Run	Resonances	Mode 1	Mode 2
1	ILR, CR, OLR	$0.48 + 0.058i$	$0.38 + 0.024i$
2	ILR, CR	$0.43 + 0.015i$	—
3	ILR, OLR	$0.49 + 0.036i$	$0.38 + 0.024i$

It can be seen that:

- All pattern speeds gained small positive biases, compared to the pattern speeds obtained from the basic integral equation (16).
- When all three terms are taken into account, both the pattern speed and the growth rate of the most unstable mode (mode 1) is determined with very good accuracy. Separate consideration of CR and OLR (runs 2 and 3) shows that the contribution of OLR term into the growth rate exceeds one of CR.
- From comparing the eigen-frequency of mode 2 obtained in runs 1 and 3, it follows that mode's growth is entirely due to the interaction of the gravitational potential of the mode with the resonance stars at OLR.

In principle, equations (54) allow to consider any number of terms, although it can be checked that the terms with $|l| \ge 2$ are of less importance. For example, taking account of terms $l = \pm 2$ will not lead to any new unstable modes. The fastest modes become rather more unstable: $\gamma_1 = 0.08$, $\gamma_2 = 0.032$.

References

[1] Arnold, V.I., 1989. *Mathematical methods of classical mechanics*, Springer.

Athanassoula, E. & Sellwood, J., 1986. *Mon. Not. Roy. Astron. Soc.*, **221**, 213.

[2] Bertin, G., Lin, C.C., 1996. *Spiral Structure in Galaxies. A density wave theory*. The MIT Press, Cambridge, Massachusetts, London, England.

[3] Binney, J., Tremaine, S., 1987. *Galactic Dynamics*. Princeton Univ. Press, Princeton, New Jersey.

[4] Blitz, L., 1983. *Science*, **220**, 1233.

[5] Case, K.M., 1960. *Phys. Fluids*, **3**, 149.

[6] Elmegreen, D.M., Elmegreen, B.G., 1982. *Mon. Not. Roy. Astron. Soc.*, **201**, 1021.

[7] Elmegreen, D.M., Elmegreen, B.G., 1987. *Astrophys. J.*, **314**, 3.

[8] Elmegreen, B.G., 1992. *Astrophys. J. Suppl. Ser.*, **79**, 37.

[9] Goldreich, P., Lynden-Bell, D., 1965. *Mon. Not. Roy. Astron. Soc.*, **130**, 125.

[10] Julian, W.H., Toomre, A., 1966. *Astrophys. J.*, **146**, 810.

[11] Kalnajs, A.J., 1965. *Ph.D. thesis*, Harvard Univ.

[12] Kalnajs, A.J., 1976. *Astrophys. J.*, **205**, 751.

[13] Kalnajs, A.J. 1978, Sympos IAU No. 77: *Structure and Properties of Nearby Galaxies*, eds.: E.M. Berhuijsen. & R. Wielebinski, p. 113.

[14] Landau, L.D. & Lifshitz, E.M., 1959. Fluid Mechanics, Pergamon, Oxford.

[15] Lin, C.C., Yuan, C., Shu, F.H., 1969. *Astrophys. J.*, **155**, 721.

[16] Lynden-Bell, D., 1979. *Mon. Not. R. astr. Soc.*, **187**, 101.

[17] Lynden-Bell, D., & Ostriker, J.P., 1967. *Mon. Not. Roy. Astron. Soc.*, **136**, 293.

[18] Lynden-Bell, D., Kalnajs, A.J., 1972. *Mon. Not. Roy. Astron. Soc.*, **157**, 1.

[19] Polyachenko, E.V., 2002a. *Mon. Not. R. astr. Soc.*, **330**, 105.

[20] Polyachenko, E.V., 2002b. *Mon. Not. R. astr. Soc.*, **331**, 394.

[21] Polyachenko, V.L., 1992. *Sov. Astron.* **36**, 5 .

[22] Polyachenko, V.L., Shukhman, I.G., 1982. *Sov. Astron.*, **26**, 140.

[23] Reed, M & Simon, B., 1972. *Method of Modern Mathematical Physics – I*, Academic Press.

[24] Sandage, A., 1961. *The Hubble Atlas of Galaxies*, Publ. No. 618. Carnegie Inst., Washington, DC.

[25] Sellwood, J.A. & Athanassoula, E., 1987. *Mon. Not. Roy. Astron. Soc.*, **229**, 707.

[26] Shu, F.H., 1970. *Astrophys. J.* **160**, 89.

[27] Toomre, A., 1969. *Astrophys. J.*, **158**, 899.

[28] Toomre, A., 1981. *in Structure and evolution of normal galaxies*. Eds.: S.M. Fall, D. Lynden-Bell. Cambridge Univ. Press. P. 111.

[29] van Kampen N.S., 1955. *Physica*, **21**, 949.